



# The effective thermal conductivity of ballistic–diffusive heat conduction in nanostructures with internal heat source



Yu-Chao Hua, Bing-Yang Cao\*

Key Laboratory for Thermal Science and Power Engineering of Ministry of Education, Department of Engineering Mechanics, Tsinghua University, Beijing 100084, China

## ARTICLE INFO

### Article history:

Received 18 May 2015

Received in revised form 21 September 2015

Accepted 22 September 2015

### Keywords:

Ballistic–diffusive heat conduction

Effective thermal conductivity

Nanostructure

Internal heat source

Phonon Boltzmann transport equation

Monte Carlo simulation

## ABSTRACT

In nanostructures whose characteristic lengths are comparable to the phonon mean free path, the ballistic–diffusive heat conduction leads to the size effect, geometry dependence and anisotropy of the effective thermal conductivity. In the present work, we have studied the effective thermal conductivity of the ballistic–diffusive heat conduction in nanostructures (including nanofilms and nanowires) with internal heat source using Monte Carlo simulation and Boltzmann transport equation. It is found that the effective thermal conductivity of nanostructures with internal heat source is significantly lower than that with temperature difference, though it still increases with the increasing characteristic length. The models for the effective thermal conductivity and the temperature distribution of the cross-plane heat conduction in the nanofilms with internal heat source are directly derived from the phonon Boltzmann transport equation, and the comparisons with the Monte Carlo simulations well confirm their validities. As for the effective thermal conductivity of the in-plane nanofilms and nanowires with internal heat source, referring to the Matthiessen's rule, the models are in the form of  $k_{eff}/k_{bulk} = 1/(1 + \alpha Kn)$ , with the parameter  $\alpha$  obtained by the best fitting with the Monte Carlo simulations. Moreover, the diffusive heat conduction equation with the effective thermal conductivity can well characterize the temperature distributions in the in-plane nanofilms and long nanowires, while it fails in the short nanowires due to the influence of the axial constraints.

© 2015 Elsevier Ltd. All rights reserved.

## 1. Introduction

Wide applications of semiconductor nanostructures in electronics and photonics require further understanding of heat transport at nanoscale [1]. Phonons predominate the heat transport in semiconductors [2]. For nanostructures whose characteristic lengths are comparable to the phonon mean free path (MFP), owing to the ballistic transport and the phonon-boundary scattering, heat conduction deviates from the Fourier's law which corresponds to the limit of completely diffusive transport. The presence of both the ballistic and diffusive transports leads to the ballistic–diffusive heat conduction which is usually characterized by the phonon Boltzmann transport equation (BTE) with the relaxation time approximation [3],

$$\vec{v}_g \cdot \nabla f = \frac{f_0 - f}{\tau} + \dot{S}_\Omega, \quad (1)$$

where  $\vec{v}_g$  is the group velocity,  $f$  is the phonon distribution function,  $f_0$  is the equilibrium distribution function,  $\tau$  is the relaxation time,

and  $\dot{S}_\Omega$  is the phonon source per solid angle. In the ballistic–diffusive regime, some of phonons can directly travel from one boundary to another without internal scattering events, and the influence of the phonon-boundary scattering becomes remarkable. Essential indications for the ballistic–diffusive heat conduction include the size effect, geometry dependence and anisotropy of the effective thermal conductivity [4–6].

Studies on the effective thermal conductivity of nanostructures have been conducted both theoretically [7–15] and experimentally [16–21]. It has been found that in the ballistic–diffusive regime the effective thermal conductivity, which significantly reduces as compared to the bulk material, increases with the increasing characteristic length and varies with the direction of heat flow. In modeling researches [7,8], a nanostructure is generally assumed to be in contact with two heat sinks of different temperatures and the temperature difference induces the heat flow. Then using the Fourier's law the effective thermal conductivity is calculated out. On the basis of the temperature difference (TD) scheme stated above, the theoretical models of the effective thermal conductivity have been derived from the phonon BTE [7–9,22]. Besides the TD scheme has been widely adopted in simulations [11,12] and experiments [4,16,17]. Actually, the TD scheme is not the only choice for the thermal

\* Corresponding author.

E-mail address: [caoby@tsinghua.edu.cn](mailto:caoby@tsinghua.edu.cn) (B.-Y. Cao).

## Nomenclature

$f$	phonon distribution function
$f_0$	equilibrium distribution function
DOS	function of phonon density of states
$l$	mean free path
$c_V$	volumetric specific heat
$v_g$	average group velocity
$Kn$	Knudsen number
$k$	thermal conductivity
$T$	temperature
$T^*$	dimensionless temperature
$q$	heat flux
$\dot{S}_\Omega$	phonon source per solid angle
$L$	length of nanowire
$D$	diameter of nanowire
$L_x$	x-directional thickness of nanofilm
$L_y$	y-directional thickness of nanofilm
$\dot{S}$	internal heat source

## Greek symbols

$\tau$	relaxation time
$\hbar$	Dirac constant
$\theta$	polar angle
$\omega$	angle frequency
$\rho$	mass density
$\varphi$	azimuthal angle
$\eta$	dimensionless coordinate

## Subscripts

0	reference state
cr	cross-plane
in	in-plane
T	temperature difference scheme
I	internal heat source scheme
film	nanofilm
wire	nanowire

conductivity measurements. The internal heat source (IHS) scheme has also been used in experiments [18–21]. The internal heat source is introduced in the nanostructures and the resulting temperature rise is measured; then the effective thermal conductivity is obtained by comparing the measuring result with the analytical solution of the diffusive heat conduction equation. Liu and Asheghi [18] measured the in-plane thermal conductivity of silicon layers by introducing a steady-state uniform internal heat source (joule heating), while the theoretical model obtained from the TD scheme was employed to analyze the experimental data. In the experiments of Johnson et al. [20], a transient internal heat source was introduced via diffraction of a laser beam to measure the thermal conductivity of the free-standing silicon membranes. In addition, the IHS scheme has also been a useful tool for the thermal conductivity measurements of carbon nanotubes [1,21].

Although both the TD and IHS schemes have been widely adopted for the thermal conductivity measurements, it is still ambiguous whether the effective thermal conductivity obtained by the TD scheme is the same as that by the IHS scheme, in particular for the ballistic-diffusive heat conduction. Li and Cao [13,14] studied the effective thermal conductivity of the nanostructures with internal heat source by the non-equilibrium molecule dynamics simulations, and found that the effective thermal conductivity in the IHS scheme was significantly lower than that in the TD scheme. Phonons emit from the heat sinks at boundaries in the TD scheme, while in the IHS scheme phonons originate within the media, and the different phonon emitting locations can lead to different boundary confined effects on phonon transport. Phonons originating within the media undergo more boundary-scatterings than these emitting from the heat sinks at the boundaries, and the mean free path (MFP) in the IHS scheme can be more confined by the boundaries than in the TD scheme [13]. According to the kinetic theory [2], the effective thermal conductivity is proportional to the boundary-confined MFP. Therefore, the effective thermal conductivity in the IHS scheme is significantly lower than that in the TD scheme. Moreover, in the electronic devices where self-heating does exist, the accurate prediction to the effective thermal conductivity of nanostructures with internal heat source becomes highly essential. Although the heat transport in electronic devices has been widely studied [23,24], the theoretical model for the effective thermal conductivity of the nanostructures with internal heat source is still lacking.

Therefore the size-dependent behavior of the effective thermal conductivity in the nanostructures with internal heat source still remains poorly understood, and the predictive model is highly desired.

In the present work, the effective thermal conductivity of the nanostructures (including nanofilms and nanowires) with internal heat source is studied. A Monte Carlo (MC) technique is applied to simulate the phonon transport. It is found that the effective thermal conductivity in the IHS scheme is significantly lower than that in the TD scheme. The predictive models for the effective thermal conductivity of the nanostructures with internal heat source are derived based on the phonon BTE and the Matthiessen's rule. Moreover, the diffusive heat conduction equation with the effective thermal conductivity is applied to characterize the temperature distributions in the nanostructures with internal heat source.

## 2. Analyses and simulation details

### 2.1. Internal heat source (IHS) scheme

The IHS scheme is illustrated in Fig. 1(a.1)–(c.1). A steady-state uniform internal heat source  $\dot{S}$  is introduced in the nanostructures in contact with two heat sinks of the reference temperature  $T_0$ . The cross sectional boundaries are adiabatic. Therefore, in the diffusive limit, the heat conduction can be regarded as one-dimensional, and the temperature profile is derived from the Fourier's law,

$$T(x) = \frac{\dot{S}}{2k}(L_x - x)x + T_0, \quad (2)$$

where  $L_x$  is the distance between the two heat sinks, and  $k$  is the thermal conductivity. Particularly, for the in-plane nanofilms as shown in Fig. 1(b.1) and the nanowires as shown in Fig. 1(c.1), the temperature  $T(x)$  is averaged in the cross-section area. The effective thermal conductivity is then extracted from the mean temperature increase  $\Delta\bar{T}$  of the nanostructures

$$k_I = \frac{L_x^2 \dot{S}}{12\Delta\bar{T}}, \quad (3)$$

with

$$\Delta\bar{T} = \frac{1}{L_x} \int_{L_x} T dx - T_0. \quad (4)$$

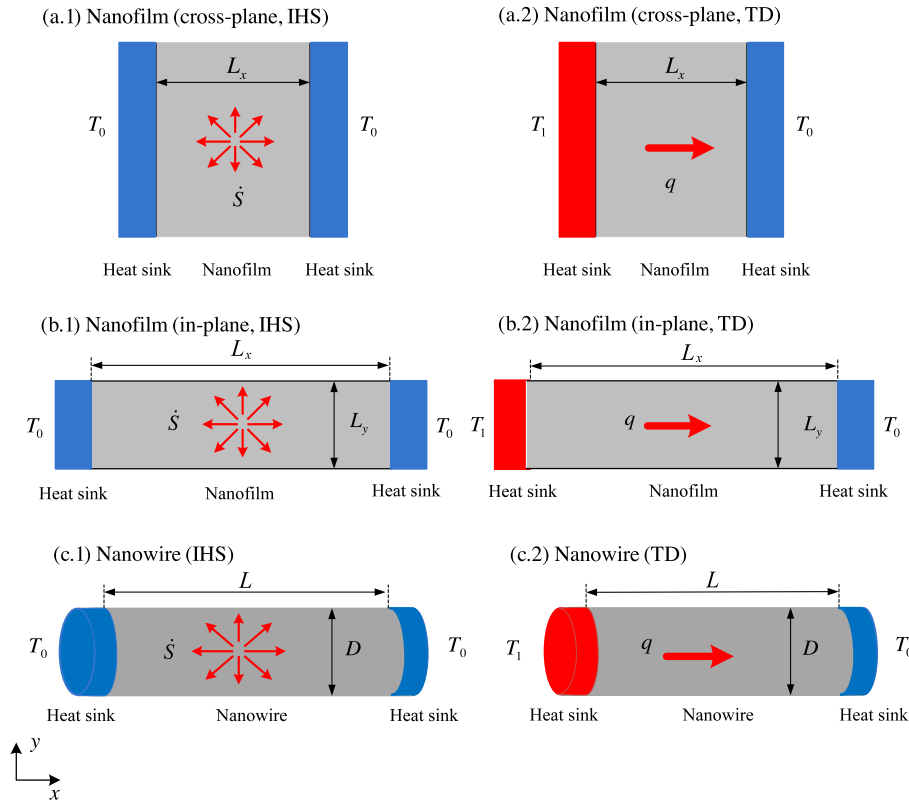


**Fig. 1.** Schematics of ballistic-diffusive heat conduction in nanostructures: (a.1) nanofilms (cross-plane, IHS); (a.2) nanofilms (cross-plane, TD); (b.1) nanofilms (in-plane, IHS); (b.2) nanofilms (in-plane, TD); (c.1) nanowires (IHS); (c.2) nanowires (TD).

## 2.2. Temperature difference (TD) scheme

In the TD scheme as shown in Fig. 1(a.2)–(c.2), each nanostructure is in contact with two heat sinks of different temperatures ( $T_1$  and  $T_0$ ), and the temperature difference is  $\Delta T = T_1 - T_0$  resulting in an  $x$ -directional heat flux  $q$ . Using the Fourier's law, the effective thermal conductivity is calculated

$$k_T = \frac{qL_x}{\Delta T}. \quad (5)$$

As for the in-plane heat conduction nanofilms as shown in Fig. 1(b.2) and the nanowires as shown in Fig. 1(c.2), the heat flux,  $q$ , is averaged in the cross-section area.

## 2.3. Monte Carlo technique

A MC technique [25–27] is applied to simulate the phonon transport in the silicon nanostructures. The gray media approximation is employed for the phonon properties of silicon, and it assumes that the phonon properties are frequency-independent. Therefore phonons travel with one group velocity and the scattering rate is described by the phonon MFP. The phonon MFP is calculated as  $l = 3k_{bulk}/(\rho c_V v_g)$ , where  $k_{bulk}$  is the bulk thermal conductivity,  $c_V$  is the volumetric specific heat,  $\rho$  is the mass density, and  $v_g$  is the average group velocity. As for silicon at room temperature,  $k_{bulk}$  is 150 W/(m K),  $c_V$  is 700 J/(kg K),  $\rho$  is 2330 kg/m<sup>3</sup>, and  $v_g$  is 6400 m/s. Thus, the phonon MFP is about 43.7 nm. Arguments still exist on the value of the phonon MFP of silicon at room temperature. Based on a more detailed dispersion model and only considering acoustic phonons that carry most of heat, the MFP of silicon is ranging from 200 nm to 300 nm [28,29]. However, when the longer MFP based on the dispersion model is

chosen, the corresponding heat capacity and group velocity should also be chosen. Here, the MFP is chosen as 43.7 nm with its corresponding specific heat and average group velocity. In fact, since all the quantities in the MC simulations and the models are dimensionless, the choice of the MFP does not influence the comparisons between them.

The MC technique is a well-developed tool for phonon heat conduction simulations. It simulates phonon transport processes by random number samplings, equivalent to directly solving the phonon BTE [25–27]. The  $x$ -directional boundaries are considered as phonon black-body, i.e., phonons are completely absorbed at them, while the lateral boundaries are adiabatic and the phonon-boundary scattering at them is assumed to be completely diffusive. As for the cross-plane heat conduction in the nanofilms, the  $y$ -directional constraints are neglected. In contrast, as for the in-plane heat conduction in the nanofilms, since the  $x$ -directional thickness is much longer than the  $y$ -directional thickness, i.e.,  $L_x \gg L_y$ , the phonon transport is mainly influenced by the  $y$ -directional boundary constraints. Similar to the in-plane heat conduction nanofilms, only the lateral constrain is considered for the long nanowires ( $L \gg D$ ), while both the lateral and axial constraints should be taken into account for the short nanowires ( $L \sim D$ ). For the TD scheme, phonons with the definite temperature emit from the heat sinks at the  $x$ -directional boundaries. In contrast, for the IHS scheme the internal heat source is implemented by setting the phonon source inside the nanostructures, that is, phonons with the definite energy originate within the nanostructures. Then phonons are traced in the domains until they exit through the  $x$ -directional boundaries, and the intrinsic scattering processes, such as phonon-impurities and phonon-phonon scatterings, are treated in the relaxation-time approximation [26]. The tracing number of phonon bundles is equal to  $10^8$ , and the unit control volume is  $\Delta x = 0.1L_x$ .

### 3. Effective thermal conductivity of nanofilms with internal heat source

#### 3.1. Cross-plane effective thermal conductivity of nanofilms

The one-dimensional phonon BTE can be applied to characterize the cross-plane phonon transport in nanofilms with internal heat source,

$$v_{gx} \frac{\partial f}{\partial x} = \frac{f_0 - f}{\tau} + \dot{S}_\Omega. \tag{6}$$

Here  $v_{gx} = v_g \cos(\theta)$ , in which  $\theta$  is the angle between the phonon traveling direction and the  $x$ -direction. The local temperature and heat flux can be derived from the integral of the distribution function

$$G(x) = 2\pi \int_{-1}^1 d\mu \int h\omega \text{DOS}(\omega) d\omega f, \tag{7}$$

$$q(x) = 2\pi \int_{-1}^1 \mu d\mu \int v_g h\omega \text{DOS}(\omega) d\omega f, \tag{8}$$

where  $\omega$  is the angle frequency of phonon,  $h$  is the Dirac constant and  $\text{DOS}(\omega)$  is the density of states. The function  $G(x)$  is directly related to the local temperature  $T(x)$ ,

$$\begin{aligned} G(x) &= 2\pi \int_{-1}^1 d\mu \int h\omega \text{DOS}(\omega) d\omega f \\ &\approx T(x) \left[ 2\pi \int_{-1}^1 d\mu \int h\omega \text{DOS}(\omega) d\omega \frac{\partial f}{\partial T} \right] \\ &\approx T(x) \left[ 2\pi \int_{-1}^1 d\mu \int h\omega \text{DOS}(\omega) d\omega \frac{\partial f_0}{\partial T} \right] = c_v \rho T(x), \end{aligned} \tag{9}$$

in which  $c_v$  is the volumetric specific heat and  $\rho$  is the mass density. When the system is comparable to the mean free path, the local thermodynamic equilibrium assumption cannot be achieved, and the temperature will lose its conventional meaning of representing a thermal equilibrium state [28]. In this case the temperature defined in Eq. (9) is a representation of the average energy of all phonons around a local point.

The distribution function can be divided into two parts,  $f = f_s + f_d$ , where  $f_s$  is the source-induced part characterized by the two-flux approximation [30] and  $f_d$  is the diffusive part characterized by the differential approximation [31]. The governing equation of the source-induced part is expressed as,

$$v_{gx} \frac{\partial f_s}{\partial x} = -\frac{f_s}{\tau} + \dot{S}_\Omega. \tag{10}$$

The two-flux approximation is employed to solve Eq. (10),

$$\begin{aligned} -\frac{1}{2} l \frac{\partial f_s^-}{\partial x} &= \tau \dot{S}_\Omega - f_s^-, \quad -1 < \mu < 0; \\ \frac{1}{2} l \frac{\partial f_s^+}{\partial x} &= \tau \dot{S}_\Omega - f_s^+, \quad 0 < \mu < +1; \end{aligned} \tag{11}$$

in which  $\mu = \cos(\theta)$ ,  $l$  is the mean free path and  $l = v_g \tau$ . With the corresponding boundary conditions:  $f_s^+(0) = 0$  and  $f_s^-(L_x) = 0$ , the source-induced part can be expressed as,

$$\begin{aligned} f_s^+(x) &= \tau \dot{S}_\Omega [1 - \exp(-2\frac{x}{l})], \\ f_s^-(x) &= \tau \dot{S}_\Omega [1 - \exp(-2\frac{L_x-x}{l})]. \end{aligned} \tag{12}$$

Thus, Eqs. (7) and (8) can be written as

$$G_s = \frac{\dot{S}}{2} \left[ 2 - \exp\left(-2\frac{x}{l}\right) - \exp\left(-2\frac{L_x-x}{l}\right) \right], \tag{13}$$

$$q_s = \frac{\dot{S}}{4} \left[ \exp\left(-2\frac{L_x-x}{l}\right) - \exp\left(-2\frac{x}{l}\right) \right], \tag{14}$$

in which  $\dot{S} = 4\pi \int h\omega \tau \dot{S}_\Omega D(\omega) d\omega$ .

As for the diffusive part, the governing equation is

$$v_g \mu \frac{\partial f_d}{\partial x} = \frac{-f_d + f_0}{\tau}. \tag{15}$$

The differential approximation assumes that [31]

$$f_d = f_d^{(0)} + \mu f_d^{(1)}. \tag{16}$$

Combining Eqs. (15) and (16), we have

$$G_d = 4\pi \int h\omega D(\omega) f_d d\omega, \tag{17}$$

$$q_d = -\frac{1}{3} l v_g \frac{\partial G_d}{\partial x}, \tag{18}$$

with the Marshak boundary conditions [31,34]:

$$\begin{aligned} \frac{G_d(0)}{4} + \frac{1}{2} q_d(0) &= 0, \\ \frac{G_d(L_x)}{4} - \frac{1}{2} q_d(L_x) &= 0. \end{aligned} \tag{19}$$

How to select the boundary condition is an important issue for the ballistic–diffusive heat conduction. For the equation of phonon radiative heat transfer Joshi and Majumdar [32] proposed the boundary condition in the form of the phonon intensity which is much similar to that applied in the heat radiation, while in the ballistic–diffusive equations Chen [31,34] obtained the Marshak boundary condition. Besides, Alvarez and Jou [33] introduced a boundary thermal resistance to deal with this issue. According to Refs. [34,35], since the boundary does not contribute to the diffusive component, the diffusive heat flux at the boundary is only made of the incident diffusive carriers. Then, the Marshak boundary condition widely adopted in the heat radiation and neutron transport can be deduced via the differential approximation [34]. In present work, the Marshak boundary condition, Eq. (19), is chosen for the diffusive component. A similar choice was made in Ofle’s work [35] where a heat radiation problem was solved by the splitting method. The ballistic transport leads to the temperature jumps at the  $x$ -directional boundaries [26], which can be characterized by Eq. (19).

According to the energy conservation equation,  $\partial q / \partial x = \dot{S}$ , we have

$$\frac{\partial q}{\partial x} = \frac{\partial q_s}{\partial x} + \frac{\partial q_d}{\partial x} = \frac{\partial q_s}{\partial x} - \frac{1}{3} l v_g \frac{\partial^2 G_d}{\partial x^2} = \dot{S}. \tag{20}$$

Combining Eqs. (14), (19) and (20), the expression of  $G_d$  is obtained,

$$\begin{aligned} G_d(x) &= \frac{3\tau}{8} \dot{S} \left[ \exp\left(-2\frac{L_x-x}{l}\right) + \exp\left(-2\frac{x}{l}\right) \right] - \frac{3\tau}{2} \dot{S} \left(\frac{x}{l}\right)^2 \\ &\quad + \frac{3\tau}{2} \dot{S} \frac{L_x}{l} \frac{x}{l} - \frac{7\tau}{8} \dot{S} + \frac{\tau}{8} \dot{S} \exp\left(-2\frac{L_x}{l}\right) + \tau \dot{S} \frac{L_x}{l}. \end{aligned} \tag{21}$$

Thus, we obtain

$$\begin{aligned} G(x) &= G_d + G_s \\ &= -\frac{\dot{S}\tau}{8} \left[ \exp\left(-2\frac{L_x-x}{l}\right) + \exp\left(-2\frac{x}{l}\right) \right] \\ &\quad + \frac{\dot{S}\tau}{8} \left[ 1 + \exp\left(-2\frac{L_x}{l}\right) \right] + \frac{3\dot{S}\tau}{2l^2} (L_x-x)x + \frac{L_x}{l} \dot{S}\tau \end{aligned} \tag{22}$$

Referring to Eq. (9), the temperature distribution function is derived from Eq. (22),

$$\begin{aligned} T_{Kn_x}^*(\eta) &= \frac{T - T_0}{(\dot{S} l_x^2 / 8k_{bulk})} = 4(1-\eta)\eta + \frac{8}{3} Kn_x \\ &\quad - \frac{Kn_x^2}{3} \left[ \exp\left(-2\frac{1-\eta}{Kn_x}\right) + \exp\left(-2\frac{\eta}{Kn_x}\right) \right] \\ &\quad + \frac{Kn_x^2}{3} \left[ 1 + \exp\left(-\frac{2}{Kn_x}\right) \right] \end{aligned} \tag{23}$$

The temperature profiles of the cross-plane heat conduction in nanofilms with internal heat source are illustrated in Fig. 2. All the quantities are converted to dimensionless: the dimensionless temperature  $T^*$  is defined as  $T^* = 8k_{bulk}(T - T_0)/(\dot{S}L_x^2)$ ; the dimensionless coordinate  $\eta$  is  $x/L_x$ ; and the Knudsen number  $Kn_x$  is defined as  $Kn_x = l/L_x$ . As  $Kn_x = 0$ , the dimensionless temperature profile corresponds to the Fourier's law, namely  $T_F^*(\eta) = 4(1 - \eta)\eta$ . The temperature jumps occur at the boundaries and increase with the increasing Knudsen number  $Kn_x$ . Besides, the dimensionless temperature increases with the increasing  $Kn_x$ , indicative of the reduction of the effective thermal conductivity. It is found that Eq. (23) can well predict the temperature distributions obtained by the MC simulations in the regime of small Knudsen number, while in the regime of large Knudsen number, owing to the violation of the differential approximation, the present model underestimates the temperature increases.

Furthermore, combining Eqs. (3) and (23) yields the model for the cross-plane effective thermal conductivity in the IHS scheme,

$$\frac{k_{I\_film\_cr}}{k_{bulk}} = \frac{1}{1 + 4Kn_x + \frac{Kn_x^2}{2} \left[ 1 + \exp\left(-\frac{2}{Kn_x}\right) \right] + \frac{Kn_x^3}{2} \left[ \exp\left(-\frac{2}{Kn_x}\right) - 1 \right]}, \quad (24)$$

with  $k_{bulk} = \rho c_V l v_g / 3$ . Majumdar [36] proposed the gray model for the cross-plane effective thermal conductivity of nanofilms in the TD scheme,

$$\frac{k_{T\_film\_cr}}{k_{bulk}} = \frac{1}{1 + \frac{4}{3}Kn_x}. \quad (25)$$

In the regime of small Knudsen number, the high order terms of  $Kn_x$  in Eq. (24) can be neglected, and it reduces to  $k_{I\_film\_cr}/k_{bulk} \approx 1/(1 + 4Kn_x)$ , which holds the same form as the gray model, i.e. Eq. (25).

Fig. 3 shows the cross-plane effective thermal conductivity of nanofilms. The effective thermal conductivity decreases with the increase of the Knudsen number  $Kn_x$  in both the IHS and TD schemes, while the effective thermal conductivity  $k_{I\_film\_cr}$  in the IHS scheme is significantly lower than  $k_{T\_film\_cr}$  in the TD scheme. Besides, the present model for  $k_{I\_film\_cr}$ , Eq. (24), agrees with the MC simulations, especially in the regime of small Knudsen number. However, as the Knudsen number increases, Eq. (24) slightly over-predicts the effective thermal conductivity.

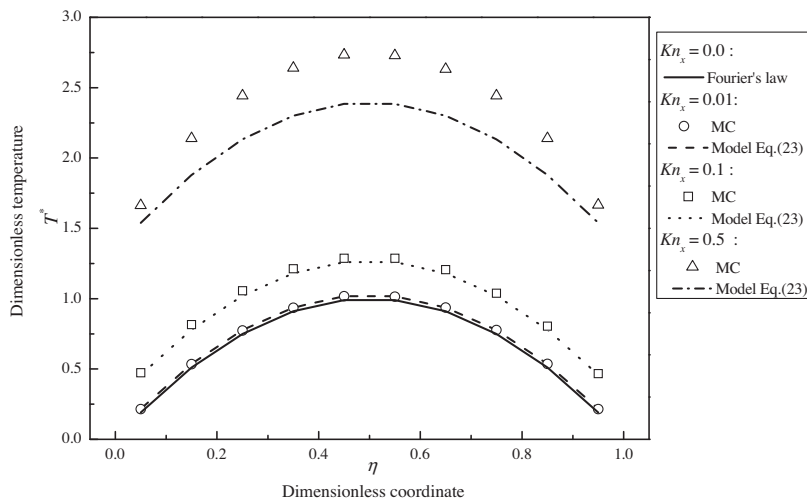


Fig. 2. Temperature distributions of cross-plane heat conduction in nanofilms with internal heat source.

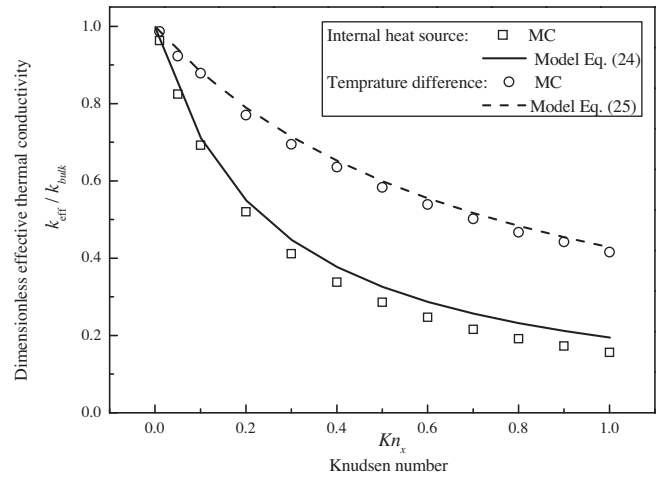


Fig. 3. Cross-plane effective thermal conductivity of nanofilms vs. Knudsen number ( $Kn_x$ ).

### 3.2. In-plane effective thermal conductivity of nanofilms

The two-dimensional phonon BTE is employed to characterize the in-plane phonon transport in nanofilms,

$$v_{gx} \frac{\partial f}{\partial x} + v_{gy} \frac{\partial f}{\partial y} = \frac{f_0 - f}{\tau} + \dot{S}_\Omega. \quad (26)$$

It is hard to derive an analytical model of the effective thermal conductivity directly from Eq. (26). Nevertheless, when the source term vanishes, Eq. (26) reduces to the governing equation in the TD scheme. The in-plane effective thermal conductivity model in the TD scheme has been derived [22]

$$\frac{k_{T\_film\_in}}{k_{bulk}} = 1 - \frac{3}{2}Kn_y \int_0^{\pi/2} \left[ 1 - \exp\left(-\frac{1}{\cos(\theta)Kn_y}\right) \right] \sin^3(\theta) d\sin(\theta), \quad (27)$$

in which  $Kn_y = l/L_y$ . It is noted that Eq. (27) can be approximately simplified as,  $k_{T\_film\_in}/k_{bulk} \approx 1/(1 + 3/8Kn_y)$  [10]. Referring to the Matthiessen's rule, we may conclude that the models of the effective thermal conductivity are in the same form,  $k_{eff}/k_{bulk} = 1/(1 + \alpha Kn)$ , in which the parameter,  $\alpha$ , reflects the size effects

under the different conditions. Hence, the form of in-plane effective thermal conductivity model in the IHS scheme is expressed as

$$\frac{k_{l\_film\_in}}{k_{bulk}} = \frac{1}{1 + \alpha_{l\_film\_in} Kn_y}, \tag{28}$$

in which the parameter  $\alpha_{l\_film\_in}$  can be obtained by the best fitting with the MC simulations. Fig. 4 illustrates the in-plane effective thermal conductivity of nanofilms varied with the Knudsen number ( $Kn_y$ ). It is found that the effective thermal conductivity decreases with the increase of  $Kn_y$  in both the TD and IHS schemes, while the effective thermal conductivity in the IHS scheme is lower than that in the TD scheme. The parameter  $\alpha_{l\_film\_in}$  for the in-plane effective thermal conductivity in the IHS scheme is equal to 0.65, calculated by the best fitting with the MC simulations in Fig. 5, and it is larger than the parameter,  $\alpha_{T\_film\_in} = 3/8$ , in the TD scheme.

Furthermore, the temperature distributions are characterized by the diffusive heat conduction equation with the effective thermal conductivity,  $k_{l\_in}$ ,

$$k_{l\_film\_in}(Kn_y) \frac{\partial^2 T}{\partial^2 x} + \dot{S} = 0. \tag{29}$$

In terms of Eq. (29), the function of the dimensionless temperature distributions within the nanofilms is

$$T_{Kn_y}^*(\eta) = 4(1 + \alpha_{l\_film\_in} Kn_y)(1 - \eta)\eta. \tag{30}$$

The dimensionless temperature distributions within the in-plane nanofilms with internal heat source are illustrated in Fig. 5. With the increase of  $Kn_y$ , owing to the  $y$ -directional boundary scattering, the dimensionless temperature increases as compared to  $T_F^*(\eta) = 4(1 - \eta)\eta$ . Since the temperature distributions still keep the parabolic form and no significant temperature jump occurs at the  $x$ -directional boundaries, Eq. (30) can well predict the temperature distributions calculated by the MC simulations.

#### 4. Effective thermal conductivity of nanowires with internal heat source

##### 4.1. Effective thermal conductivity of long nanowires

Firstly, we consider the long nanowires in which the influence of the axial constraints can be neglected, and the effective thermal

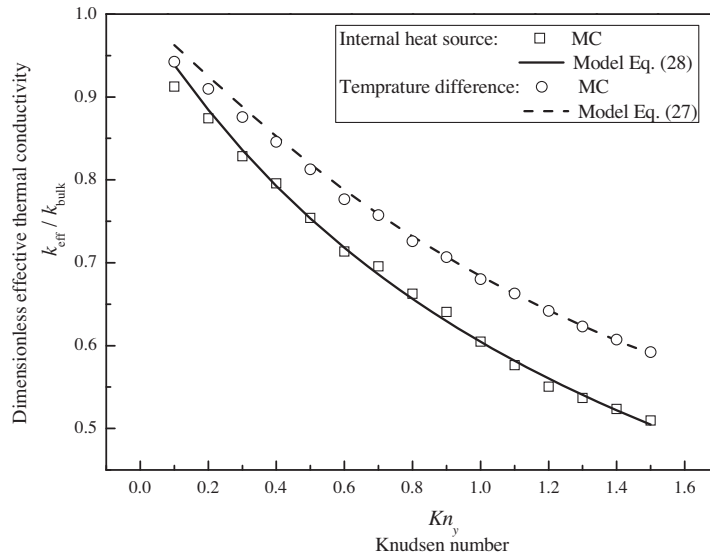


Fig. 4. In-plane effective thermal conductivity of nanofilms vs. Knudsen number ( $Kn_y$ ).

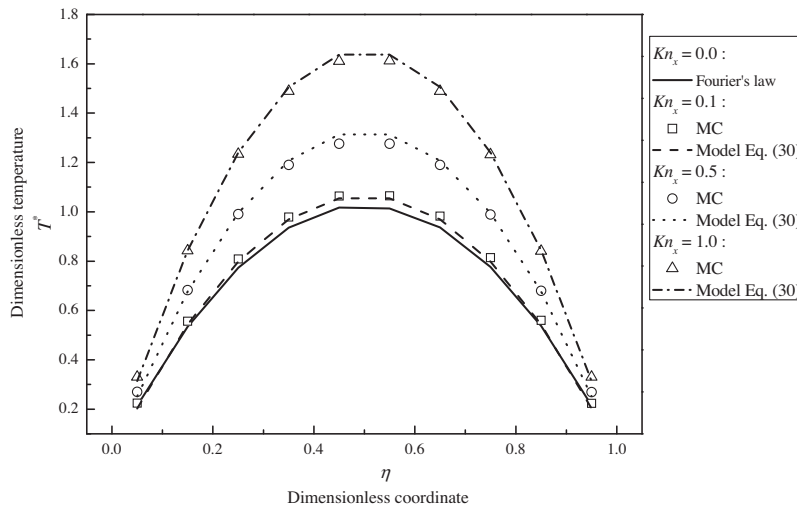


Fig. 5. Temperature distributions of in-plane heat conduction in nanofilms with internal heat source.

conductivity only depends on the diameter ( $D$ ) of the nanowires. The corresponding Knudsen number,  $Kn_D$ , is then defined as  $Kn_D = l/D$ . Similar to the in-plane effective thermal conductivity of the nanofilms, the model for the long nanowires with internal heat source is in the form of

$$\frac{k_{I\_wire}}{k_{bulk}} = \frac{1}{1 + \alpha_{I\_wire\_D} Kn_D}, \tag{31}$$

where  $\alpha_{I\_wire\_D}$  can be obtained by the best fitting with the MC simulations. As a comparison, the model in the TD scheme is derived from the phonon BTE without internal heat source [8],

$$\frac{k_{T\_wire}}{k_{bulk}} = 1 - \frac{3}{\pi} \int_0^1 r dr \int_0^{2\pi} \int_0^1 \exp\left(-\frac{1}{2Kn_D} \frac{\sin(\varphi - \arcsin(r \sin(\varphi)))}{\sin(\varphi)\sqrt{1-\mu^2}}\right) \mu^2 d\mu d\varphi, \tag{32}$$

which can be approximately simplified as,  $k_{T\_wire}/k_{bulk} \approx 1/(1 + 3/4Kn_D)$  [10].

Fig. 6 shows the effective thermal conductivity of the long nanowires varied with the Knudsen number ( $Kn_D$ ). Eq. (32) well agrees with our MC simulations in the TD scheme. The parameter,

$\alpha_{I\_wire\_D}$ , in the IHS scheme is calculated as 1.26, larger than the parameter,  $\alpha_{T\_wire\_D} = 3/4$ , in the TD scheme. Besides, the effective thermal conductivity decreases with the increase of  $Kn_D$  in both the above schemes, while the effective thermal conductivity,  $k_{I\_wire}$ , in the IHS scheme is significantly lower than  $k_{T\_wire}$  in the TD scheme.

The diffusive heat conduction equation with the effective thermal conductivity is applied to characterize the temperature distributions in the long nanowires with internal heat source,

$$T_{Kn_D}^*(\eta) = 4(1 + \alpha_{I\_wire} Kn_D)(1 - \eta)\eta. \tag{33}$$

Fig. 7 shows the dimensionless temperature distributions within the long nanowires with internal heat source. It is found that the temperature increases as compared to that predicted by the Fourier's law, though it still holds the parabolic form and no significant boundary temperature jump occurs. Therefore, Eq. (33) can well agree with the MC simulations.

#### 4.2. Effective thermal conductivity of short nanowires

When the influence of the axial constraints cannot be neglected, the effective thermal conductivity of the short nanowires depends on both the diameter  $D$  and the length  $L$ . Referring to

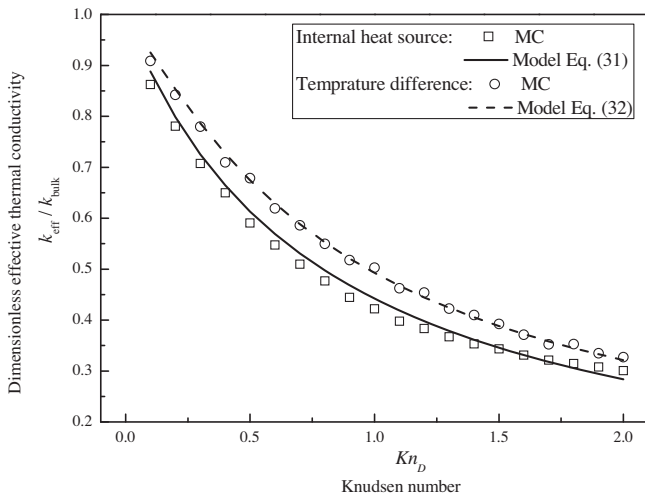


Fig. 6. Effective thermal conductivity of long nanowires vs. Knudsen number ( $Kn_D$ ).

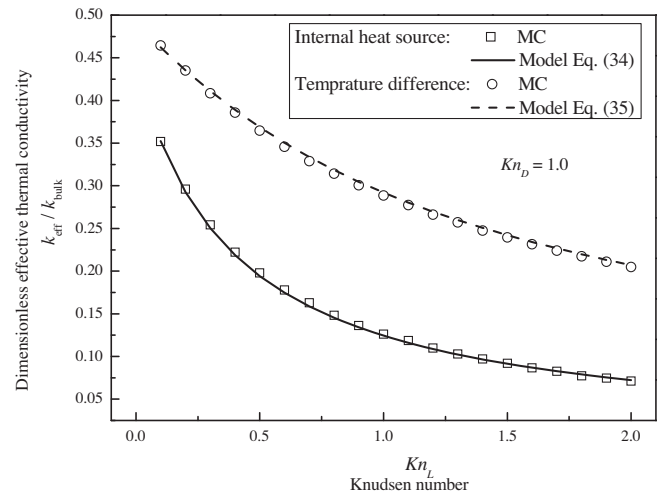


Fig. 8. Effective thermal conductivity of short nanowires vs. Knudsen number ( $Kn_L$ ).

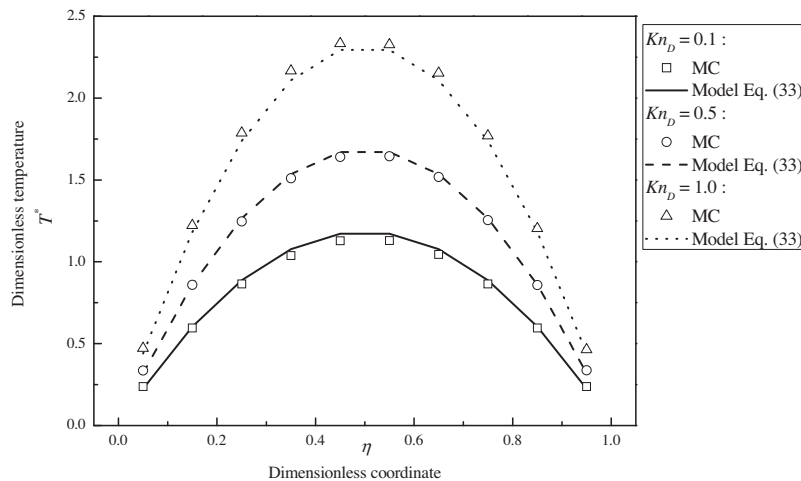


Fig. 7. Temperature distributions in long nanowires with internal heat source.

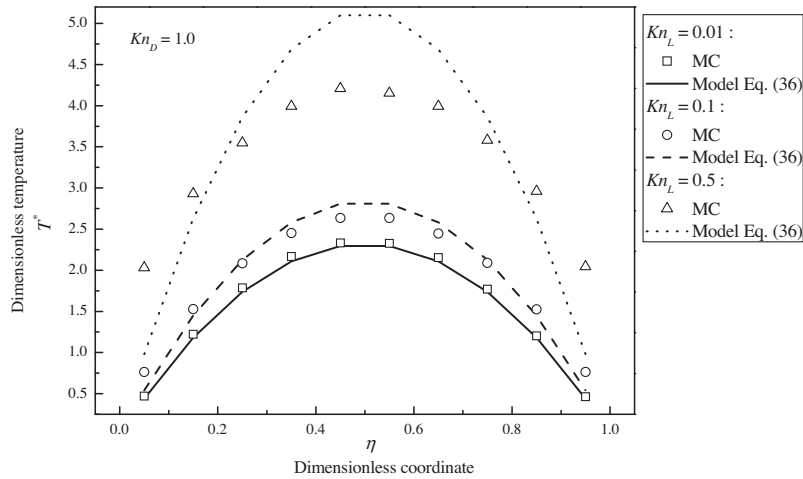


Fig. 9. Temperature distributions in short nanowires with internal heat source.

the Matthiessen’s rule, the corresponding effective thermal conductivity model for the short nanowires may be expressed as

$$\frac{k_{I\_wire}}{k_{bulk}} = \frac{1}{1 + \alpha_{I\_wire\_D}Kn_D + \alpha_{I\_wire\_L}Kn_L} \quad (34)$$

Here  $\alpha_{I\_wire\_D} = 1.26$  which is obtained in Section 4.1 for the long nanowires, and the parameter  $\alpha_{I\_wire\_L}$  is obtained by the best fitting with the MC simulations in Fig. 8. Besides, in the TD scheme, the effective thermal conductivity model of the short nanowires is [37]

$$\frac{k_{T\_wire}}{k_{bulk}} = \frac{1}{\frac{4}{3}Kn_L + \left(1 - \frac{3}{\pi} \int_0^1 r dr \int_0^{2\pi} \int_0^1 \exp\left(-\frac{\sin(\varphi - \arcsin(r \sin(\varphi)))}{2Kn_D \sin(\varphi) \sqrt{1-\mu^2}}\right) \mu^2 d\mu d\varphi\right)^{-1}} \quad (35)$$

Fig. 8 shows the effective thermal conductivity of short nanowires. Eq. (35) well predicts the effective thermal conductivity calculated by the MC simulations in the TD scheme. The parameter,  $\alpha_{I\_wire\_L}$ , in the IHS scheme is calculated as 5.78. In addition, the effective thermal conductivity of short nanowires is lower than that of long nanowires, owing to the influence of axial constraints. With the increase of length, the effective thermal conductivity increases. Besides, like the long nanowires, the effective thermal conductivity of short nanowires in the IHS scheme is also significantly lower than that in the TD scheme.

The diffusive heat conduction equation with the effective thermal conductivity of the short nanowires is expressed as

$$T_{(Kn_D, Kn_L)}^*(\eta) = 4(1 + \alpha_{I\_wire\_D}Kn_D + \alpha_{I\_wire\_L}Kn_L)(1 - \eta)\eta. \quad (36)$$

As shown in Fig. 9, in the regime of large  $Kn_L$ , owing to the influence of the  $x$ -directional constraints, the temperature distributions within the short nanowires calculated by the MC simulations significantly deviate from the parabolic form and the temperature jumps occur at the boundaries. Hence different from the long nanowires, Eq. (36) cannot well predict the temperature distributions within the short nanowires in the regime of large  $Kn_L$ .

5. Conclusions

We have studied the effective thermal conductivity of nanostructures (including nanofilms and nanowires) with internal heat source. A Monte Carlo technique is applied to simulate the phonon transport in the nanostructures. It is found that the effective thermal conductivity of nanostructures with internal heat source is sig-

Table 1 Parameters for effective thermal conductivity models.

		The TD scheme	The IHS scheme
Nanofilm	Cross-plane	4/3	4
	In-plane	3/8	0.65
Nanowire	Diameter dependence	3/4	1.26
	Length dependence	4/3	5.78

nificantly lower than that with temperature difference, though it still increases with the increasing characteristic length.

The models of the effective thermal conductivity and the temperature distribution for the cross-plane nanofilm heat conduction with internal heat source are directly derived from the phonon Boltzmann transport equation, and the comparisons with the Monte Carlo simulations well confirm their validities.

Referring to the Matthiessen’s rule, the models for the effective thermal conductivity of nanofilms and nanowires can be simplified as the unified form of,  $k_{eff}/k_{bulk} = 1/(1 + \alpha Kn)$ . Particularly for short nanowires, the effective thermal conductivity model is expressed as  $k_{eff}/k_{bulk} = 1/(1 + \alpha_L Kn_L + \alpha_D Kn_D)$ , taking into account the multiple constraints. The parameters for the different geometries in both the TD and IHS schemes are illustrated in Table 1.

The diffusive heat conduction equation with the effective thermal conductivity is applied to characterize the temperature distributions within the nanofilms and nanowires,  $k_{I\_eff}(Kn)\partial^2 T/\partial^2 x + \dot{S} = 0$ . As for the in-plane nanofilms and long nanowires, the above equation can well predict the temperature distributions. However, as for the short nanowires in which the axial constraints cannot be neglected, since the temperature distributions deviate from the parabolic form and the temperature jumps occur at the  $x$ -directional boundaries, the above equation fails to predict the temperature distributions.

Conflict of interest

None declared.

Acknowledgements

This work is financially supported by National Natural Science Foundation of China (Nos. 51322603, 51136001, 51356001), Program for New Century Excellent Talents in University, and Science Fund for Creative Research Group (No. 51321002).

## References

- [1] E. Pop, Energy dissipation and transport in nanoscale devices, *Nano Res.* 3 (2010) 147–169.
- [2] J. Ziman, *Electrons and Phonons*, Oxford University Press, London, 1961. pp. 1–61.
- [3] D.G. Cahill, P.V. Braun, G. Chen, et al., Nanoscale thermal transport. II. 2003–2012, *Appl. Phys. Lett.* 1 (2014) 011305.
- [4] R. Chen, A.I. Hochbaum, P. Murphy, et al., Thermal conductance of thin silicon nanowires, *Phys. Rev. Lett.* 101 (2008) 105501.
- [5] R.B. Wilson, D.G. Cahill, Anisotropic failure of Fourier's theory in time-domain thermoreflectance experiments, *Nat. Commun.* 5 (2014) 5075.
- [6] J. Chen, G. Zhang, B. Li, A universal gauge for thermal conductivity of silicon nanowires with different cross sectional geometries, *J. Chem. Phys.* 135 (2011) 204705.
- [7] G. Chen, C.L. Tien, Thermal conductivities of quantum well structures, *J. Thermophys. Heat Tr.* 7 (1993) 311–318.
- [8] X. Lü, W.Z. Shen, J.H. Chu, Size effect on the thermal conductivity of nanowires, *J. Appl. Phys.* 91 (2002) 1542–1552.
- [9] A. Sellitto, F.X. Alvarez, D. Jou, Geometrical dependence of thermal conductivity in elliptical and rectangular nanowires, *Int. J. Heat Mass Trans.* 55 (2012) 3114–3120.
- [10] A.J.H. McGaughey, E.S. Landry, D.P. Sellan, et al., Size-dependent model for thin film and nanowire thermal conductivity, *Appl. Phys. Lett.* 99 (2011) 131904.
- [11] S.C. Wang, X.G. Liang, X.H. Xu, et al., Thermal conductivity of silicon nanowire by nonequilibrium molecular dynamics simulations, *J. Appl. Phys.* 105 (2009) 014316.
- [12] D. Lacroix, K. Joulain, D. Lemonnier, Monte Carlo transient phonon transport in silicon and germanium at nanoscales, *Phys. Rev. B* 72 (2005) 064305.
- [13] Y.W. Li, B.Y. Cao, Thermal conductivity of single-walled carbon nanotube with internal heat source studied by molecular dynamics simulation, *Int. J. Thermophys.* 34 (2011) 2361–2370.
- [14] B.Y. Cao, Y.W. Li, A uniform source-and-sink scheme for calculating thermal conductivity by nonequilibrium molecular dynamics, *J. Chem. Phys.* 133 (2010) 024106.
- [15] D.P. Sellan, J.E. Turney, A.J.H. McGaughey, et al., Cross-plane phonon transport in thin films, *J. Appl. Phys.* 108 (2010) 113524.
- [16] D. Li, Y. Wu, P. Kim, et al., Thermal conductivity of individual silicon nanowires, *Appl. Phys. Lett.* 83 (2003) 2934–2936.
- [17] T.K. Hsiao, H.K. Chang, S.C. Liou, et al., Observation of room-temperature ballistic thermal conduction persisting over 8.3 microm in SiGe nanowires, *Nat. Nanotechnol.* 8 (2013) 534–538.
- [18] W. Liu, M. Asheghi, Phonon-boundary scattering in ultrathin single-crystal silicon layers, *Appl. Phys. Lett.* 84 (2004) 3819–3821.
- [19] W. Liu, M. Asheghi, Thermal conductivity measurements of ultra-thin single crystal silicon layers, *J. Heat Trans.* 128 (2006) 75–83.
- [20] J.A. Johnson, A.A. Maznev, J. Cuffe, et al., Direct measurement of room-temperature nondiffusive thermal transport over micron distances in a silicon membrane, *Phys. Rev. Lett.* 110 (2013) 025901.
- [21] V. Deshpande, S. Hsieh, A. Bushmaker, et al., Spatially resolved temperature measurements of electrically heated carbon nanotubes, *Phys. Rev. Lett.* 102 (2009) 105501.
- [22] X. Wang, B. Huang, Computational study of in-plane phonon transport in Si thin films, *Sci. Rep.* 4 (2014) 6399.
- [23] E. Pop, R.W. Dutton, K.E. Goodson, Monte Carlo simulation of Joule heating in bulk and strained silicon, *Appl. Phys. Lett.* 86 (2005) 082101.
- [24] R. Yang, G. Chen, M. Laroche, et al., Simulation of nanoscale multidimensional transient heat conduction problems using ballistic-diffusive equations and phonon Boltzmann equation, *J. Heat Trans.* 127 (2005) 298–306.
- [25] J.P.M. Péraud, N.G. Hadjiconstantinou, An alternative approach to efficient simulation of micro/nanoscale phonon transport, *Appl. Phys. Lett.* 101 (2012) 153114.
- [26] Y.C. Hua, B.Y. Cao, Phonon ballistic-diffusive heat conduction in silicon nanofilms by Monte Carlo simulations, *Int. J. Heat Mass Trans.* 78 (2014) 755–759.
- [27] Y.C. Hua, Y. Dong, B.Y. Cao, Monte Carlo simulation of phonon ballistic diffusive heat conduction in silicon nanofilm, *Acta Phys. Sin.* 62 (2013) 244401.
- [28] G. Chen, Thermal conductivity and ballistic-phonon transport in the cross-plane direction of superlattices, *Phys. Rev. B* 57 (1998) 14958.
- [29] E. Pop, K.E. Goodson, Heat generation and transport in nanometer-scale transistors, *Proc. IEEE* 94 (2006) 1587–1601.
- [30] M.F. Modest, *Radiative Heat Transfer*, Academic press, 2003.
- [31] G. Chen, Ballistic-diffusive heat-conduction equations, *Phys. Rev. Lett.* 86 (2001) 2297–2300.
- [32] A.A. Joshi, A. Majumdar, Transient ballistic and diffusive phonon heat transport in thin films, *J. Appl. Phys.* 74 (1993) 31–39.
- [33] F.X. Alvarez, D. Jou, Boundary conditions and evolution of ballistic heat transport, *J. Heat Trans.* 132 (2010) 012404.
- [34] G. Chen, Ballistic-diffusive equations for transient heat conduction from nano to macroscales, *J. Heat Trans.* 124 (2002) 320–328.
- [35] D. Olfe, A modification of the differential approximation for radiative transfer, *AIAA J.* 5 (1967) 638–643.
- [36] A. Majumdar, Microscale heat conduction in dielectric thin films, *J. Heat Trans.* 115 (1993) 7–16.
- [37] Y.C. Hua and B.Y. Cao, Ballistic-diffusive heat conduction in multiply-constrained nanostructures, 2015 (Submitted to *International Journal of Thermal Sciences*).